NeuroImage: Clinical 37 (2023) 103303

Contents lists available at ScienceDirect

NeuroImage: Clinical

journal homepage: www.elsevier.com/locate/ynicl

Gray to white matter signal ratio as a novel biomarker of neurodegeneration in Alzheimer's disease

Deepti Putcha [a,c,1,*], Yuta Katsumi [a,b,1,*], Michael Brickhouse [a,b], Ryn Flaherty [a,b], David H. Salat [d,e,g], Alexandra Touroutoglou [a,b,f,2,*], Bradford C. Dickerson [a,b,c,e,f,2]

[a] Frontotemporal Disorders Unit, Massachusetts General Hospital and Harvard Medical School, Boston, MA, USA
[b] Department of Neurology, Massachusetts General Hospital and Harvard Medical School, Boston, MA, USA
[c] Department of Psychiatry, Massachusetts General Hospital and Harvard Medical School, Boston, MA, USA
[d] Department of Radiology, Massachusetts General Hospital and Harvard Medical School, Boston, MA, USA
[e] Athinoula A. Martinos Center for Biomedical Imaging, Massachusetts General Hospital and Harvard Medical School, Boston, MA, USA
[f] Massachusetts Alzheimer's Disease Research Center, Massachusetts General Hospital and Harvard Medical School, Boston, MA, USA
[g] Neuroimaging Research for Veterans Center, VA Boston Healthcare System, Boston, MA, USA

ARTICLE INFO

Keywords:
Cortical atrophy
Microstructure
Tau
Amyloid
Magnetic resonance imaging
Positron emission tomography

ABSTRACT

Alzheimer's disease (AD) is characterized neuropathologically by β-amyloid (Aβ) plaques, hyperphosphorylated tau neurofibrillary tangles, and neurodegeneration, which lead to a phenotypically heterogeneous cognitive-behavioral dementia syndrome. Our understanding of how these neuropathological and neurodegeneration biomarkers relate to each other is still evolving. A relatively new approach to measuring structural brain change, gray matter to white matter signal intensity ratio (GWR), quantifies the signal contrast between these tissue compartments, and has emerged as a promising marker of AD-related neurodegeneration. We sought to validate GWR as a novel MRI biomarker of neurodegeneration in 29 biomarker positive individuals across the atypical syndromic spectrum of AD. Bivariate correlation analyses revealed that GWR was associated with cortical thickness, tau PET, and amyloid PET, with GWR showing a larger magnitude of abnormality than cortical thickness. We also found that combining GWR, cortical thickness, and amyloid PET better explained observed tau PET signal than using these modalities alone, suggesting that the three imaging biomarkers contribute independently and synergistically to explaining the variance in the distribution of tau pathology. We conclude that GWR is a uniquely sensitive *in vivo* marker of neurodegenerative change that reflects pathological mechanisms which may occur prior to cortical atrophy. By using all of these imaging biomarkers of AD together, we may be better able to capture, and possibly predict, AD neuropathologic changes *in vivo*. We hope that such an approach will ultimately contribute to better endpoints to evaluate the efficacy of therapeutic interventions as we move toward an era of disease-modifying treatments for this devastating disease.

1. Introduction

Alzheimer's disease (AD) is characterized neuropathologically by β-amyloid (Aβ) plaques, hyperphosphorylated tau neurofibrillary tangles, and neurodegeneration (Hyman et al., 2012), which lead to a phenotypically heterogeneous cognitive-behavioral dementia syndrome. The ATN classification system, which focuses on *in vivo* biomarkers to identify the presence or absence of amyloid (A), tau (T), and neurodegeneration (N) in each individual (Jack et al., 2018), has been a useful research framework. However, our understanding of how biomarkers of these neuropathologic features relate to each other is still growing. Magnetic resonance imaging (MRI) biomarkers of the neurodegenerative component of AD—most commonly MRI-based cortical thickness (Dickerson et al., 2009) or volumetric measurements—may be limited in their sensitivity to detect early pathology given that atrophy typically follows amyloid and tau spread (Jack et al., 2013). Additionally, regional brain atrophy is non-specific, also reflecting non-AD pathological processes such as vascular disease (Wirth et al., 2013) or

* Corresponding authors at: Frontotemporal Disorders Unit, Massachusetts General Hospital and Harvard Medical School, Boston, MA, USA.
E-mail addresses: dputcha@mgh.harvard.edu (D. Putcha), ykatsumi@mgh.harvard.edu (Y. Katsumi), atouroutoglou@mgh.harvard.edu (A. Touroutoglou).
[1] Equal contributions as co-first authors.
[2] Equal contributions as co-senior authors.

https://doi.org/10.1016/j.nicl.2022.103303
Received 19 September 2022; Received in revised form 21 December 2022; Accepted 22 December 2022
Available online 24 December 2022

other co-occurring pathologies (Brenowitz et al., 2017). There is a critical need to improve the sensitivity and specificity of measurements of cerebral structural integrity in order to better inform diagnosis, prognostication, and outcomes monitoring.

A relatively new approach to measuring structural brain change relevant to aging and AD has focused on MRI-based tissue signal properties. The gray matter to white matter signal intensity ratio (GWR), which quantifies the signal contrast between these tissue compartments, has emerged as a promising marker of AD-related neurodegeneration that can be measured using conventional MRI scans. Reports indicate that a decrease in the contrast between the tissue classes is observed with increasing disease severity. Changes in GWR have been reported with a spatial pattern associated with traditional markers of neurodegeneration, including cortical atrophy in "AD-signature" regions in the medial and lateral temporal cortex, posterior cingulate, and precuneus in individuals with amnestic AD (Salat et al., 2011; Westlye et al., 2009). Abnormal GWR also tracks with scores on the Clinical Dementia Rating (CDR) scale (Grydeland et al., 2013; Jefferson et al., 2015; Salat et al., 2011). GWR appears—at least from cross-sectional analyses—to sensitively identify brain regions in the early stages of the illness that develop atrophy subsequently as the illness progresses (Salat et al., 2011), although there is no longitudinal evidence to date that has confirmed this hypothesis. Critically, these earlier studies demonstrated that GWR signal changes were observed even after controlling for changes in morphometric properties (i.e., the effects of AD on GWR went beyond cortical atrophy or volume loss alone), suggesting that GWR is a uniquely sensitive *in vivo* microstructural marker of neurodegenerative change in AD and may reflect pathological mechanisms that occur prior to cortical atrophy (Salat et al., 2011).

Although GWR may reflect disease severity, there has not yet been an investigation of how GWR signal is related to AD molecular neuropathic changes (regional amyloid and tau deposition). Furthermore, no investigation of GWR to date has examined atypical syndromes of AD—Posterior Cortical Atrophy (PCA; the visual variant) and logopenic variant of Primary Progressive Aphasia (lvPPA; the language variant), which are characterized by neurodegenerative spatial topographies different from typical amnestic AD. In the current study, we sought to validate GWR as a novel MRI biomarker of neurodegeneration in A+/T+/N + individuals across the symptomatic atypical syndromic spectrum of AD. To do this, we examined the relationships between signal from GWR, MRI-based cortical thickness, amyloid PET, and tau PET. We then used GWR, cortical thickness, and amyloid PET as predictor variables to investigate how these measures would explain the variance in the spatial distribution of tau PET signal. We hypothesized that the topography of GWR would be overlapping but not identical to the topography of cortical atrophy observed in our patients with atypical AD. Based on prior work suggesting that GWR and cortical thickness may reflect distinct neurobiological mechanisms (Grydeland et al., 2013; Westlye et al., 2010), we also expected that GWR and cortical atrophy would be associated with tau PET signal in different regions relevant to the various stages of AD progression. Specifically, we expected to see spatial overlap between GWR and tau PET signal in prefrontal cortical regions which are thought to represent regions with faster tau accumulation as the disease progresses (Sintini et al., 2019). In contrast, we did not expect to see this spatial overlap between cortical atrophy and tau PET in prefrontal cortical regions, given our previous observations of cortical atrophy in predominantly posterior cortical regions in this patient sample at this level of disease severity (Putcha et al., 2019). Since the topography of amyloid PET signal generally does not reflect syndromic variability and does not reliably co-localize with regions of neurodegeneration at this stage of disease progression (Day et al., 2017; Putcha et al., 2019; Xia et al., 2017), we hypothesized weaker relationships between both measures of neurodegeneration (GWR and cortical atrophy) and amyloid PET signal compared with tau PET signal. Finally, we hypothesized that GWR and cortical thickness would have partially independent and complementary effects on explaining regional variability in tau PET signal.

2. Methods

2.1. Participants

Twenty-nine amyloid-, tau-, and neurodegeneration positive (A+/T+/N +) (Jack et al., 2016) individuals with atypical variants of AD were included in this study, all of whom were recruited from the Massachusetts General Hospital (MGH) Frontotemporal Disorders Unit Primary Progressive Aphasia (Sapolsky et al., 2010) and Posterior Cortical Atrophy (Putcha et al., 2018; Wong et al., 2019) programs (Table 1). All participants received a standard clinical evaluation comprising a structured history obtained from both patient and informant to inform clinician scoring on the CDR, comprehensive neurological and psychiatric history and exam, and neuropsychological assessment. All were administered the Montreal Cognitive Assessment (MoCA), a brief screening tool for cognitive impairment covering domains of orientation, executive functions, visuospatial cognition, memory, and language (Nasreddine et al., 2005). The total score on this test was calculated out of the maximum of 30; the means and standard deviations of our sample are included in Table 1. Clinical diagnostic formulation was performed through consensus conference by our multidisciplinary team of neurologists, neuropsychologists, and speech and language pathologists, with each patient classified based on all available clinical information as having a 3-step diagnostic formulation of mild cognitive impairment or dementia (Cognitive Functional Status), a specific Cognitive-Behavioral Syndrome, and a likely etiologic neuropathologic diagnosis (Dickerson et al., 2017). Regarding cognitive-behavioral syndrome, 16 individuals met diagnostic criteria for Posterior Cortical Atrophy (PCA) (Crutch et al., 2017; Mendez et al., 2002; Tang-Wai et al., 2004), 10 met criteria for logopenic variant primary progressive aphasia (lvPPA) (Gorno-Tempini et al., 2011), and three individuals met criteria for a dysexecutive variant of Alzheimer's disease (Ossenkoppele et al., 2015; Townley et al., 2020). All individuals underwent neuroimaging sessions which included structural MRI, ^{11}C-Pittsburgh Compound B (PiB) PET, and ^{18}F-flortaucipir (FTP) PET scans. Aβ positivity was determined by visual read according to previously published procedures (Rabinovici et al., 2010) as well as a summary distribution volume ratio (DVR) of frontal, lateral temporoparietal, and retrosplenial (FLR) regions >1.2 (Villeneuve et al., 2015). Determination of tau and neurodegeneration positivity was conducted also by visual read using internal methods

Table 1
Demographic and clinical characteristics of the sample.

Demographics	All patients (n = 29)	PCA (n = 16)	lvPPA (n = 10)	Dysexecutive (n = 3)	Aβ- CN (n = 24)
Age (years)	69.2 ± 7.6	68.4 ± 8.5	71.0 ± 6.1	66.7 ± 8.1	67.4 ± 4.9
Sex (M/F)	17/12	6/10	4/6	2/1	12/12
Education (years)	16.9 ± 2.7	16.3 ± 2.9	17.4 ± 2.7	18.0 ± 0	†15.7 ± 2.3
MoCA	17.7 ± 5.8	20.4 ± 6.4	14.2 ± 3.7	19.5 ± 0.7	–
CDR	CDR 0.5 (N = 18) CDR 1 (N = 10) CDR 2 (N = 1)	CDR 0.5 (N = 9) CDR 1 (N = 6) CDR 2 (N = 1)	CDR 0.5 (N = 8) CDR 1 (N = 2)	CDR 0.5 (N = 1)CDR 1 (N = 2)	–
CDR-SOB	3.8 ± 2.2	4.5 ± 2.4	2.7 ± 1.4	3.8 ± 1.6	–
PiB FLR DVR	1.90 ± 0.3	1.87 ± 0.3	1.92 ± 0.3	1.97 ± 0.2	1.11 ± 0.05

Note: MoCA = Montreal Cognitive Assessment. CDR = Clinical Dementia Rating scale. SOB = Sum of Box scores. PiB FLR DVR = Pittsburgh Compound B Fronto-Lateral-Retrosplenial Distribution Value Ratio. †Data based on n = 13.

similar to published work (e.g., Fleisher et al., 2020; Rabinovici et al., 2011; Sonni et al., 2020).

We included a group of amyloid-negative (Aβ-) cognitively normal (CN) individuals, all of whom performed within normal limits on neuropsychological testing, had normal brain structure based on MRI, and low cerebral amyloid based on quantitative analysis of PiB PET data (FLR DVR < 1.2), resulting in a CN sample of 24 individuals (see Table 1). This control sample was used as a reference for quantifying elevated signal in each modality in our patients. Individuals were excluded from our patient and control groups if they had a primary psychiatric or other neurologic disorder including major cerebrovascular infarct or stroke, seizure, brain tumor, hydrocephalus, multiple sclerosis, HIV-associated cognitive impairment, or acute encephalopathy. This work was carried out in accordance with The Code of Ethics of the World Medical Association (Declaration of Helsinki) for experiments involving humans. All participants and their informants/caregivers provided informed consent in accordance with the protocol approved by the MassGeneral Brigham HealthCare System Human Research Committee Institutional Review Board in Boston, Massachusetts.

2.2. Neuroimaging data acquisition and preprocessing

Structural MRI data were acquired from each participant on a Siemens Tim Trio 3.0 Tesla scanner using a T1-weighted multi-echo magnetization prepared rapid acquisition sequence (MEMPRAGE) (repetition time = 2530 ms, echo times = 1.64/3.5/5.36/7.22 ms, flip angle = 7°, slice thickness = 1 mm, field of view = 256 mm, 0 % slice gap). Each participant's MEMPRAGE data underwent intensity normalization, skull stripping, and an automated segmentation of cerebral white matter to locate the gray matter/white matter boundary via FreeSurfer v6.0, which is documented and freely available for download online (https://surfer.nmr.mgh.harvard.edu). Defects in the surface topology were corrected (Fischl et al., 2001), and the gray/white boundary was deformed outward using an algorithm designed to obtain an explicit representation of the pial surface. We visually inspected each participant's cortical surface reconstruction for technical accuracy and manually edited it when necessary. Cortical thickness was calculated as the closest distance from the gray/white boundary to the gray/CSF boundary at each vertex on the tessellated surface (Fischl & Dale, 2000). The ratio of gray to white matter signal intensity (GWR) was calculated for each vertex based on white matter signal intensity (W) sampled at 1 mm subjacent to the gray-white interface as well as gray mater signal intensity (G) sampled at 30 % through the thickness of the cortical ribbon normal to the gray/white border, using the following formula:

$$GWR = \frac{100 \times (W - G)}{0.5 \times (W + G)}$$

W and G were measured at these locations to be (1) relatively close to one another while minimizing partial volume effects and (2) not crossing surfaces (e.g., going too far into white matter and ending up in gray matter). While these parameters were not derived empirically, they have proven to be sensitive in prior studies of GWR (e.g., Salat et al., 2009, 2011). Whole-brain maps of cortical thickness and GWR were registered to a template surface (fsaverage) and smoothed geodesically with full-width-half-maximum (FWHM) of 10 mm.

All participants underwent FTP and PiB PET scans. The FTP radiotracer was prepared at MGH with a radiochemical yield of 14 ± 3 % and specific activity of 216 ± 60 GBq/μmol (5837 ± 1621 mCi/μmol) at the end of synthesis (60 min) and validated for human use (Shoup et al., 2013). The PiB radiotracer was prepared as described previously (Becker et al., 2011). All PET data were acquired using a Siemens (Knoxville, TN) ECAT HR + scanner: 3D mode, 63 imaging planes, 15.2 cm axial field of view, 5.6 mm transaxial resolution, and 2.4 mm slice interval. FTP PET images were acquired from 80 to 100 min after a 10.0 ± 1.0 mCi bolus injection in 4 × 5 min frames. PiB PET images were acquired with an 8.5 to 10.5 mCi bolus injection followed immediately by a 60 min dynamic acquisition in 69 frames (12 × 15 *sec*, 57 × 60 *sec*). All PET data were reconstructed and attenuation corrected; each frame was evaluated to verify adequate count statistics and interframe head motion was corrected.

We performed further processing of FTP and PiB PET data via the PetSurfer tools (Greve et al., 2014, 2016). Each participant's PET data were first rigidly coregistered to their anatomical volume and the accuracy of cross-modal spatial registration was confirmed by visual inspection. PET data were then corrected for partial volume effects. Specifically, based on each participant's high-resolution tissue segmentation derived by the standard Desikan-Killiany atlas (Desikan et al., 2006), the symmetric geometric transfer matrix (GTM) method was used to correct for spill-in and spill-out effects between adjacent brain tissue types, with a point spread function of 6 mm (Greve et al., 2014, 2016). Using partial volume-corrected data, we derived the FTP and PiB standard uptake value ratio (SUVR) image per participant with whole cerebellar gray matter as a reference region (Johnson et al., 2016). Non-partial volume corrected PiB SUVR maps were also used to derive FLR DVR for the confirmation of Aβ positivity. FTP and PiB SUVR maps were resampled to fsaverage space and smoothed geodesically with FWHM of 8 mm.

To identify areas of the cerebral cortex showing elevated signal in each modality and in each AD patient, we calculated a vertex-wise W-score map (Katsumi et al., 2022a,b; Putcha et al., 2022). W-scores are analogous to Z-scores adjusted for specific covariates of no interest, which in this study were age and sex. Briefly, we first performed a vertex-wise multiple regression analysis using surface maps of cortical thickness, GWR, FTP SUVR, and PiB SUVR obtained from Aβ- CN participants, which resulted in whole-cortex beta coefficient maps of age and sex as well as individual maps of residuals for each modality. We then computed W-scores for each patient and at each vertex using the following formula:

$$W = \frac{Y - \widehat{Y}}{SD_{residuals}}$$

where Y = the observed signal for a given patient and modality, $\widehat{Y}$ = the predicted signal for a given modality based on age and sex of a given patient as well as beta coefficients obtained from Aβ- CN participants, and $SD_{residuals}$ = the standard deviation of the individual residual maps for a given modality obtained from Aβ- CN participants.

2.3. Statistical analysis

Using individual cortical thickness, GWR, FTP SUVR, and PiB SUVR maps as inputs, we first created a series of whole-cortex vertex-wise general linear models (GLM) in FreeSurfer to identify areas of the cerebral cortex where AD patients showed abnormal signal in each modality than Aβ- CN participants. To quantify signal abnormality in each modality, we derived a vertex-wise map of effect size (Cohen's d) calculated as the difference in group means divided by the pooled standard deviation at each vertex.

To investigate the relationships across modalities, we reduced the dimensionality of group-level W-score maps into 400 cortical regions based on an established functional parcellation (Schaefer et al., 2018), which has been spatially mapped to canonical functional networks of the cerebral cortex (Yeo et al., 2011). For a given pair of modalities, we then computed the Pearson's correlation coefficient to examine the strength of bivariate association at the group level. In addition, we secondarily performed similar bivariate correlation analyses separately for each functional network and for each cerebral cortical lobe by focusing on a subset of cortical parcels. Functional network assignment was determined by the original network labels provided by Schaefer et al. (2018), which consisted of the following: Visual, Somatomotor, Dorsal Attention, Ventral Attention, Limbic, Frontoparietal, and Default. Lobar

assignment was determined using vertex-wise labels based on the PALS-B12 atlas available in FreeSurfer: Frontal, parietal, limbic, temporal/insular, and occipital.

Finally, we constructed linear mixed-effects models (LMEMs) to test the relative contribution of each non-FTP modality to explaining the variance in regional FTP uptake. LMEMs included all cortical regions from all individual patients as observations (400 parcels × 29 patients), with FTP as the dependent variable. We tested a total of seven models with one for each non-FTP modality, one for each pairwise combination, and the full model including all fixed predictors. Random intercepts and slopes for patients were included in all models. Detailed model specifications are as follows:

Model 1 (cortical thickness only):

FTP ~ 1 + cortical thickness + (1 + cortical thickness | patient).

Model 2 (GWR only):

FTP ~ 1 + GWR + (1 + GWR| patient).

Model 3 (PiB only):

FTP ~ 1 + PiB + (1 + PiB | patient).

Model 4 (cortical thickness and GWR):

FTP ~ 1 + cortical thickness + GWR + (1 + cortical thickness + GWR | patient).

Model 5 (cortical thickness and PiB):

FTP ~ 1 + cortical thickness + PiB + (1 + cortical thickness + PiB | patient).

Model 6 (GWR and PiB):

FTP ~ 1 + GWR + PiB + (1 + GWR + PiB | patient).

Model 7 (cortical thickness, GWR, and PiB):

FTP ~ 1 + cortical thickness + GWR + PiB + (1 + cortical thickness + GWR + PiB | patient).

All LMEMs were constructed and tested using the *lme4* package (Bates et al., 2015) run on R v4.2.1 and used the restricted maximum likelihood method for parameter estimation. To statistically compare performance between a given pair of models, we refit each model with maximum likelihood estimation and conducted a likelihood ratio test. All variables were converted to *Z*-scores prior to model fitting.

3. Results

3.1. Demographic and clinical characteristics.

Table 1 reports the demographic and clinical characteristics of our sample including the A+/T+/N + AD patients and Aβ- CN participants. Regarding cognitive functional status, the patients included in this study were largely either classified as having mild cognitive impairment (CDR = 0.5) or mild dementia (CDR = 1), with the majority of patients (18/29) in this study rated at the stage of mild cognitive impairment. All were highly educated, and on average performed at a level of moderate impairment on the MoCA. All individuals in this sample self-reported their race to be non-Hispanic White.

3.2. AD biomarkers of neurodegeneration and neuropathology are distinct but overlapping

We first aimed to investigate the similarities and differences across our four metrics of interest: Cortical thickness and GWR representing traditional and novel metrics of AD-related neurodegeneration, as well as FTP PET and PiB PET, representing neuropathological tau and amyloid deposition, respectively (Fig. 1). We found that, when examined at the same threshold (Cohen's $d > 1.5$), GWR was prominently abnormal in widespread areas of the cerebral cortex whereas abnormal cortical thickness was minimally observed. At a more liberal threshold (Cohen's $d > 0.75$), cortical thickness showed abnormal signal mainly in lateral temporoparietal and medial parietal cortical regions, which spatially overlapped with the topography of abnormal GWR signal (see also Supplementary Fig. 1). GWR—but not cortical thickness—was abnormal in lateral and medial prefrontal cortices (PFC), which were observed in our maps of neuropathological tau (FTP) and amyloid (PiB) deposition as well. A secondary analysis was performed to examine the topography of abnormal signal in each modality separately for each AD clinical phenotype group (PCA, lvPPA, and dysexecutive AD). This analysis showed that, as was the case with the whole group analysis, GWR signal was more prominently abnormal than cortical thickness in the medial and lateral prefrontal areas in each clinical phenotype group (Supplementary Figs. 2–4), thus suggesting that the spatial topography of GWR signal abnormality is highly replicable across AD phenotype groups.

Abnormal FTP PET signal, reflecting hyperphosphorylated tau deposition, was robustly observed in posterior cortical regions with modest lateral PFC involvement, while abnormal PiB PET signal, reflecting fibrillar amyloid deposition, was prominent in much more widespread cortical areas, including the frontal cortex. Abnormal GWR signal was co-localized with abnormal FTP PET signal in lateral PFC regions, with only minimal co-localized abnormalities in cortical thickness. Abnormal GWR signal was also co-localized with abnormal PiB PET signal in PFC regions. These observations suggest that abnormal

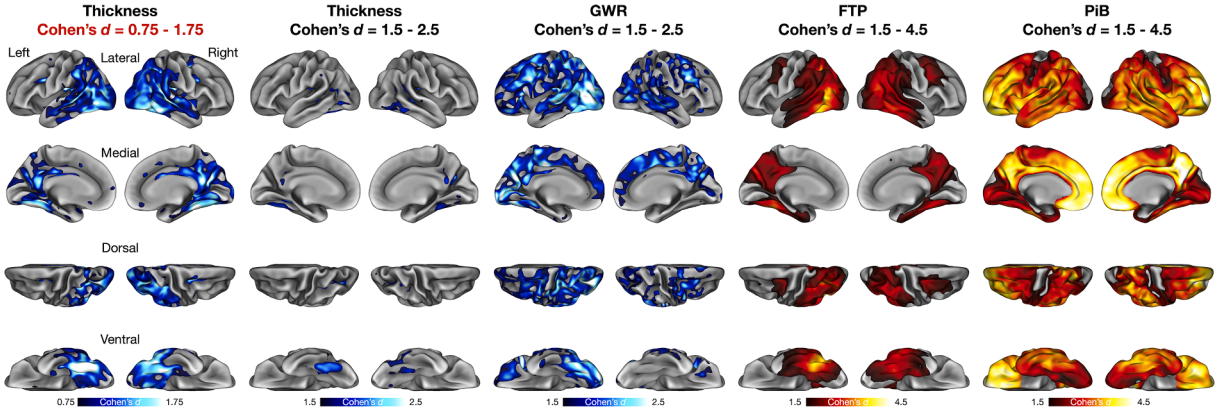

Fig. 1. Whole-cortex maps of multimodal AD-related imaging biomarkers. Group-level effect size (Cohen's *d*) maps show signal abnormalities in AD patients relative to controls of cortical thickness, GWR, FTP PET, and PiB PET. When examined at the same threshold ($d > 1.5$), GWR exhibits more prominent abnormality than cortical thickness in widespread areas of the cerebral cortex. When a more lenient threshold is used to examine cortical thickness ($d > 0.75$), GWR and cortical thickness, two distinct T1-weighted MRI markers of neurodegeneration, demonstrate abnormal signal overlap in lateral temporoparietal and medial parietal cortical regions, with GWR demonstrating substantially larger effect sizes. GWR additionally shows abnormal signal in lateral and medial prefrontal cortices. Two *in vivo* measures of neuropathology show a greater dissociation: FTP PET signal, reflecting hyperphosphorylated tau deposition, is observed more heavily in posterior cortical regions with modest lateral prefrontal involvement, while PiB PET signal, reflecting amyloid deposition, is prominent in more widespread areas, including the frontal lobe.

GWR may reflect similar aspects of neurodegeneration as those measured by abnormal cortical thickness (albeit with greater sensitivity) in posterior cortical regions, and it may also be more sensitive to concurrent neuropathological protein deposition and potentially future sites of atrophy. For the interested reader, vertex-wise maps depicting mean cortical thickness, GWR, FTP PET, and PiB PET signal separately for AD patients and Aβ-CN participants are provided in Supplementary Material (Supplementary Figs. 5–8).

3.3. Bivariate relationships between measures of neurodegeneration and neuropathology

To clarify the relationships between these structural MRI biomarkers of neurodegeneration (cortical atrophy and GWR) and PET biomarkers measuring tau (FTP) and amyloid (PiB) across the atypical syndromic spectrum of AD, we parcellated data in each modality (*W*-scores) into 400 nodes and plotted bivariate correlations at the group level (Fig. 2); the color of each node represents its assignment to a canonical functional network of the cerebral cortex as defined by Yeo et al. (2011). Unsurprisingly, we observed a moderate correlation between cortical thickness and GWR (Fig. 2A; $r = 0.36$, $p < .001$). This suggests that although they are both structural MRI biomarkers of neurodegeneration, they may be sensitive to different aspects of AD neuropathologic changes. We observed the strongest relationship between cortical thickness and FTP (Fig. 2B; Pearson's $r = -0.79$, $p < .001$), such that regions with the highest tau burden also had greatest atrophy. We also observed a strong relationship between GWR and FTP (Fig. 2C; $r = -0.56$, $p < .001$), such that regions with the highest tau burden showed reduced T1-weighted MRI contrast between gray and white matter signal. Visual inspection of these bivariate associations led to the observation that, in the somatomotor network, there was abnormal GWR signal in the context of low tau, which weakened the magnitude of the GWR-FTP relationship at the whole group/parcellation level compared with the thickness-FTP relationship (Fig. 2C). Once we removed the parcels belonging to this network, the relationship between GWR and FTP became stronger in magnitude (Supplementary Figure 9). The other relationships involving PiB PET were weaker in magnitude (Fig. 2D-2F).

The pattern of bivariate associations between cortical thickness, GWR, FTP, and PiB was generally replicable at the level of individual patients (Supplementary Fig. 10) and within each clinical phenotype of AD (Supplementary Figs. 11–13). Moreover, these correlations were also similarly identified at the level of individual functional networks (Supplementary Fig. 14–20). The relationship between cortical thickness and FTP was consistently strong in every network, whereas the bivariate relationships involving GWR or PiB were more variable across networks. A similar pattern was also observed when bivariate correlations were examined in each cerebral cortical lobe (Supplementary Fig 21–25).

3.4. GWR explains FTP signal variability after controlling for cortical thickness

Table 2 reports results from linear mixed-effects models (LMEMs) predicting regional FTP uptake. We found that cortical thickness (Model 1), GWR (Model 2), and PiB (Model 3) all predict FTP signal

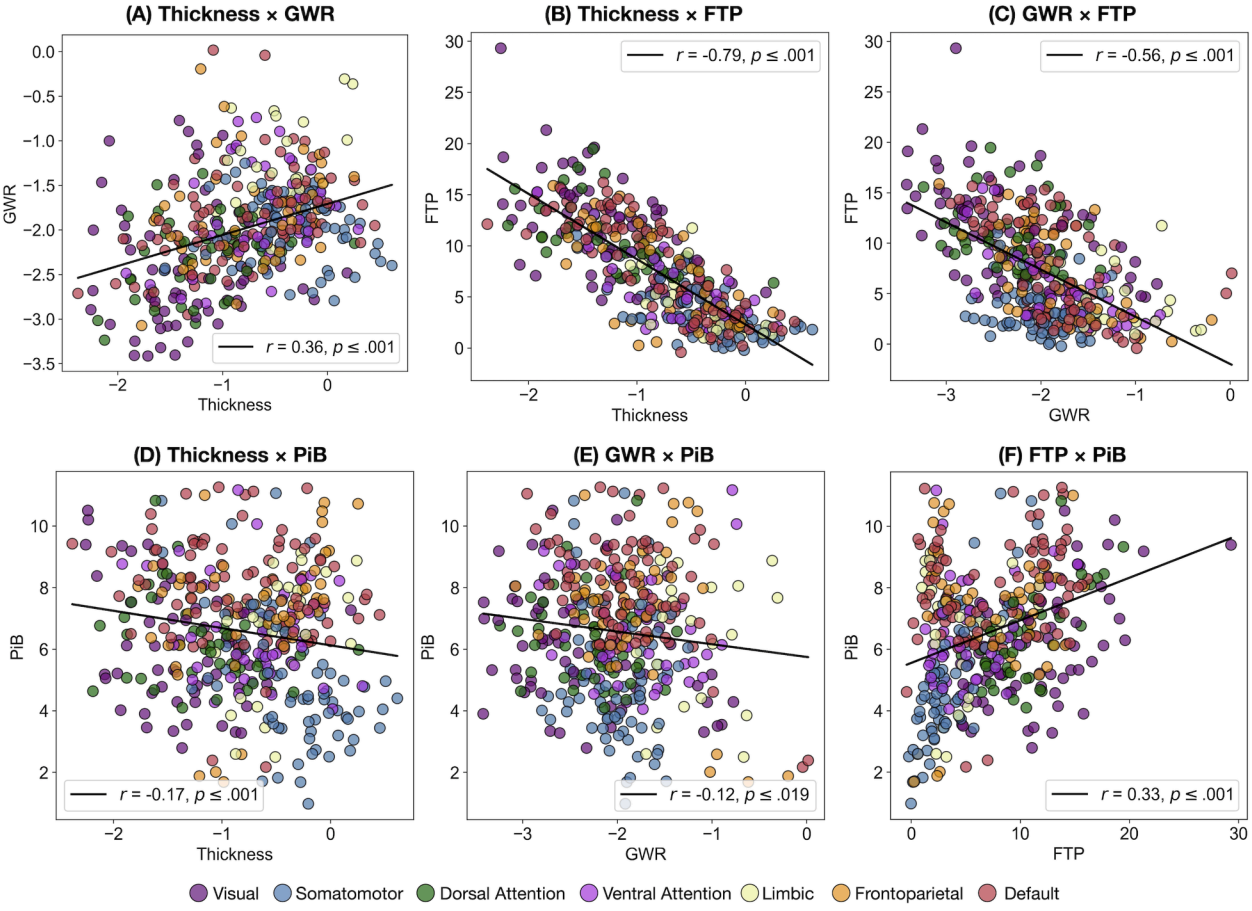

Fig. 2. Bivariate relationships between GWR, Cortical Thickness, FTP, and PiB. *W*-score maps of signal from each MRI and PET measure were parcellated into 400 nodes and plotted against each other. Pearson's *r* correlation coefficients were calculated to determine the strength of bivariate correlations at the group level. The color of each node represents its assignment to a canonical functional network of the cerebral cortex as defined by Yeo et al. (2011). Cortical thickness and FTP showed the strongest relationship to each other, followed by GWR and FTP. Cortical thickness and GWR showed a modest relationship to each other, with PiB showing an even weaker association with each MRI measure.

Table 2

Linear mixed-effects models (LMEMs) predicting regional FTP uptake. LMEMs included all cortical regions from all individual patients as observations (400 parcels × 29 patients), with FTP PET signal as the dependent variable. All variables were converted to *Z*-scores across all observations prior to model fitting. Fixed effects parameter estimates (with standard error in parentheses) are reported with statistical significance denoted at various levels: $^{*}p < .05$, $^{**}p < .01$, $^{***}p < .001$. For each model, the following goodness-of-fit statistics were computed: The Akaike Information Criterion (AIC), marginal R^2 (proportion of variance explained by the fixed effect factors), conditional R^2 (proportion of variance explained by the fixed and random factors), and Root Mean Square Error (RMSE). We tested a total of seven models with one for each non-FTP modality (Model 1: cortical thickness, Model 2: GWR, Model 3: PiB), one for each pairwise combination (Model 4: GWR and cortical thickness, Model 5: PiB and cortical thickness, Model 6: PiB and GWR), and the full model including all fixed predictors (Model 7). Random intercepts and slopes for patients were included in all models. The model including all three predictors of FTP (Model 7) was the strongest in explaining observed FTP signal (highest marginal R^2), suggesting that cortical thickness, GWR, and PiB all contribute unique information in predicting tau pathology.

	Model 1	Model 2	Model 3	Model 4	Model 5	Model 6	Model 7
Fixed Effects							
(Intercept)	0.002 (0.083)	0.036 (0.133)	0.015 (0.102)	0.010 (0.112)	0.055 (0.116)	0.025 (0.133)	0.050 (0.131)
Cortical thickness	-0.566 (0.040)***			-0.490 (0.033)***	-0.522 (0.037)***		-0.450 (0.031)***
GWR		-0.556 (0.056)***		-0.332 (0.038)***		-0.501 (0.051)***	-0.305 (0.036)***
PiB			0.373 (0.067)***		0.317 (0.057)***	0.345 (0.057)***	0.311 (0.048)***
Fit Statistics							
AIC	25531.3	28081.7	28669.8	24,243	23660.8	26183.3	**22476.6**
Marginal R^2	0.297	0.199	0.112	0.319	0.299	0.254	**0.331**
Conditional R^2	0.519	0.585	0.455	0.649	0.679	0.668	0.743
RMSE	0.72	0.8	0.82	0.68	0.66	0.73	0.62

independently, with cortical thickness showing the strongest relationship with FTP followed by GWR, reflecting our results from the bivariate correlation analysis reported above. When we examined pairwise combinations, we found that GWR explains additional variance in FTP signal after controlling for cortical thickness (Model 4), as revealed by a likelihood ratio test identifying better fit for Model 4 than Model 1:

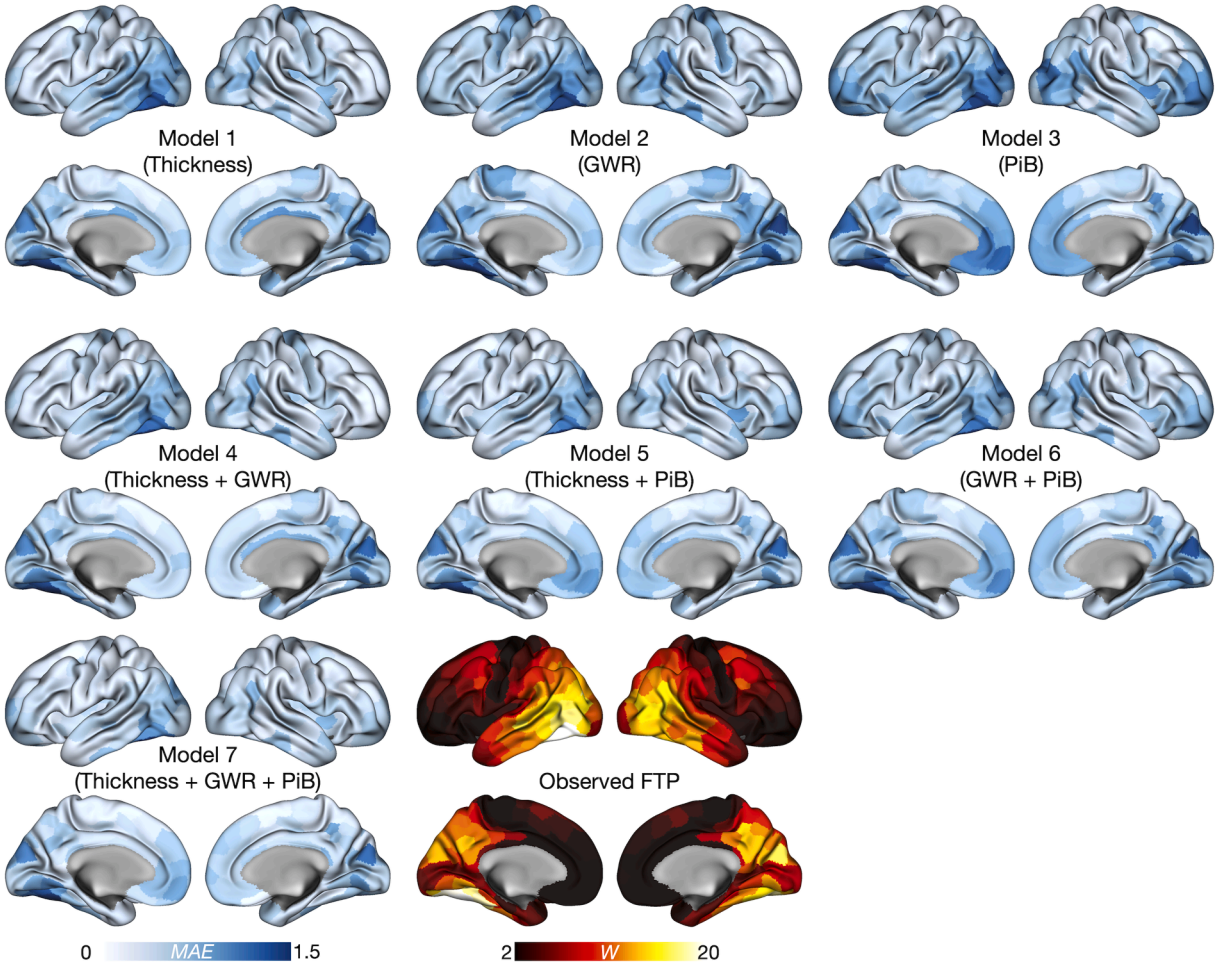

Fig. 3. Parcel-wise linear mixed effects model residuals depicted topographically on the cortical surface. Across the whole cortex, lighter colors closer to white represent smaller mean absolute error (MAE) for each parcel indicating superior model performance, while darker blue colors represent greater error in predicting observed FTP. Model 7 including all three predictors of tau shows the best fit (the least MAE, consistent with the lowest AIC as well as the largest marginal R^2 estimate as reported in Table 2). (For interpretation of the references to color in this figure legend, the reader is referred to the web version of this article.)

$\chi^2(4) = 1300.9$, $p < .001$. PiB also contributed unique variance to explaining FTP signal after controlling for cortical thickness (Model 5), yielding better fit than Model 1: $\chi^2(4) = 1882.1$, $p < .001$. When GWR and PiB were tested as predictors, both metrics contributed uniquely to explaining FTP signal (Model 6), with GWR signal observed to be more strongly related to FTP. Lastly, we found that the model including all three predictors (Model 7) explained the largest variance in observed FTP signal, statistically outperforming Model 4 ($\chi^2(4) = 1780.7$, $p < .001$), Model 5 ($\chi^2(4) = 1199.6$, $p < .001$), and Model 6 ($\chi^2(4) = 3723.3$, $p < .001$). This suggests that cortical thickness, GWR, and PiB all contribute unique information in predicting tau pathology. This effect is visualized in Fig. 3, which depicts the data presented in Table 2 topographically on the cortical surface with lighter colors representing reduced mean absolute error and darker blue colors representing greater error.

3.5. Effect of partial volume correction.

To investigate the effect of partial volume correction on our PET data, we repeated the same analyses discussed above using non-partial volume corrected FTP and PiB data. Overall, we obtained similar results regardless of whether partial volume correction was involved, with a slight decrease in the parameter estimates and an increase in the goodness-of-fit statistics in our LMEMs when non-partial volume corrected data were used (Supplementary Figs. 26 and 27; Supplementary Table 1). These results suggest that partial volume correction had a minimal impact on driving our findings, and if anything, it appears to provide a small boost in model performance.

4. Discussion

Our ability to study the heterogeneous phenotypic spectrum of AD has greatly improved since the advent of *in vivo* molecular biomarkers of AD neuropathologic changes, and our understanding of the relationships between amyloid and tau PET signal with structural MRI measures is evolving. MRI measures of regional brain atrophy are co-localized with hyperphosphorylated tau and the magnitude of abnormalities in these two elements of AD pathophysiology are strongly correlated, supporting observations from studies of post-mortem brain tissue (Gómez-Isla et al., 1997). This evidence suggests that cerebral atrophy (presumably reflecting neuronal loss, at least in part) is tightly coupled with neurofibrillary and neuritic tau pathology. The results of our study show that GWR—a relatively new MRI-based biomarker of tissue properties measurable from the same T1-weighted sequence as regional brain volume—appears to offer information complementary to volumetrics regarding the pathological effects of amyloid and tau on brain structure. As such, GWR is a novel MRI biomarker of AD-related neurodegeneration.

In this study, we investigated GWR in biomarker-confirmed (A+/T+/N +) individuals across the atypical syndromic spectrum of AD, which offers the opportunity to examine dissociations in the spatial topography of imaging biomarkers. Consistent with previous reports in amnestic AD (Salat et al., 2011; Westlye et al., 2009), we found that abnormal GWR is closely co-localized with abnormal cortical thickness in posterior cortical areas, but that the abnormalities in GWR are of much greater magnitude in those regions and extend beyond them. This evidence suggests that GWR may be a more sensitive metric of neurodegeneration than cortical thickness, possibly enabling detection of changes in microstructural properties that cannot be captured by traditional cortical morphometric measures (Salat et al., 2011). For example, it is possible that decreased GWR reflects changes in the neuropil such as synaptic loss and gliosis that occur prior to the emergence of cell loss which is presumably the major driver of gray matter atrophy. We also observed dissociations between these two measures of neurodegeneration: While cortical atrophy was minimal in the PFC, GWR was prominently reduced in the lateral and medial PFC. Bivariate correlational analyses also revealed only a modest correlation between GWR and cortical thickness, further supporting the idea that the extent to which these measures show divergent sensitivity may depend on specific areas of the cerebral cortex.

Previous studies also demonstrated that abnormalities of GWR were present in areas that were not atrophic, suggesting that GWR may be a uniquely sensitive microstructural biomarker of neurodegenerative change in AD and may reflect pathological mechanisms that occur prior to cortical atrophy (Salat et al., 2011). We tested this hypothesis cross-sectionally by examining whether GWR and cortical thickness relate differently to molecular neuropathological biomarkers of amyloid and tau. We found that abnormal GWR was present in some brain regions where there was elevated tau PET signal but minimal cortical atrophy, reinforcing the hypothesis that GWR may become abnormal in relation to tau pathology prior to atrophy. In addition, abnormal GWR was present in the medial PFC where there was elevated amyloid PET signal but neither tau nor cortical atrophy, suggesting that GWR may also be sensitive to amyloid pathology at least in some regions. Supporting this observation, the bivariate association between GWR and PiB PET became stronger in magnitude when examined in a regionally-specific manner (e.g., in the limbic lobe and the default mode network including part of the medial PFC). The strength of this association between GWR and PiB PET also exceeded that of the association between cortical thickness and PiB PET in these regions critical to AD. At the more general, whole-cortex level, however, cortical thickness was comparably or more strongly associated with FTP and PiB than GWR. More research is therefore needed to systematically characterize the regional specificity of GWR's sensitivity to amyloid accumulation. As anticipated, the relationships between amyloid PET and cortical thickness, GWR, and tau PET were relatively weak, consistent with the idea that amyloid deposition precedes abnormal signal in these other biomarkers throughout the pathological cascade of AD and may plateau in the early symptomatic phase of AD, while the other biomarkers continue to increase as symptoms progress. Critical to our hypothesis that these two structural MRI measures provide unique information about pathological processes in AD, we found that GWR signal explained additional variance in tau PET signal over and above cortical thickness measurements. Taken together, these observations suggest that GWR is more sensitive than cortical thickness to some aspects of neurodegeneration, likely capturing local changes in these two tissue compartments in earlier stages of AD. When used in conjunction, GWR and cortical thickness may help enhance sensitivity in detecting AD-related neuropathological changes, while also providing specificity for different processes depending on the relative involvement of microstructural and macrostructural effects, respectively. Furthermore, GWR may reflect amyloid-related changes in tissue properties and may precede future sites of atrophy, although this hypothesis remains to be directly tested in longitudinal investigations. Based on our results from linear mixed effects modeling of these different measurement modalities, we suggest that using GWR in addition to volumetrics may shed new light on diagnosis, prognosis, and monitoring. This will be of particular interest in amyloid-related disease-modifying clinical trials, where it will be important to examine whether GWR diverges from volumetric measures in an informative way as amyloid is cleared from cerebral tissue.

Our study has some limitations that would be important to address, which we hope will inspire future research endeavors to better understand and utilize GWR in studies of neurodegenerative diseases. First, our study focused on a relatively small sample of atypical AD cases, as these understudied individuals demonstrate heterogeneous topographies of AD-related tau and neurodegeneration. Future studies could expand this work to examine the full syndromic range of AD, including the typical amnestic variant. In the current study, we did not observe evidence of model singularity even with the most complex model structure, suggesting that statistically there was no indication of model overfitting. However, a larger and more heterogeneous sample would be useful in further minimizing the risk of overfitting in future work.

Furthermore, most of our participants were at stages of mild cognitive impairment and mild dementia. We may gain a better understanding of how the relationships between these imaging biomarkers in AD evolve with a broader clinical range of disease severity inclusive of preclinical individuals through moderate dementia. Additionally, the cross-sectional nature of this study and its implications for our conclusions postulating GWR as a harbinger of future pathological change need to be directly substantiated with longitudinal investigation. The results reported here suggest that GWR is observed in regions where tau PET signal is abnormal (e.g., PFC) and may represent sites of future tau accumulation and atrophy. Longitudinal analyses would be additionally useful in directly testing our hypothesized spatiotemporal trajectories of the relationships between neuropathological and neurodegeneration biomarkers and how they relate to changes in disease severity. Moreover, given that GWR was found to be complementary to cortical thickness in explaining tau accumulation, further research is warranted to clarify what neurodegenerative processes GWR may be a proxy for. For instance, examination of the relationship between GWR and regional hypometabolism as measured by ^{18}F-fluorodeoxyglucose (FDG) PET would be particularly useful, as the latter has been shown to be more strongly correlated with FTP PET signal than cortical thickness in AD (Whitwell et al., 2018). Cortical hypometabolism has also been shown to appear before cortical atrophy in AD (Kljajevic et al., 2014). Finally, it would be important for future studies to further investigate the relationship between GWR and amyloid deposition by, for example, examining how GWR can be used to differentiate Aβ + individuals from Aβ- individuals. Recent evidence identifies alterations in cortical microstructural properties (as estimated by diffusion MRI) in AD, which were associated with the pattern of amyloid accumulation (Spotorno et al., 2022). Future studies should thus clarify the associations between GWR and other metrics microstructural integrity, with the goal to identify their common and dissociable sensitivity to neuropathological processes.

In summary, we demonstrate that GWR is a promising measure to better understand the neurodegenerative component of the A/T/N framework used to characterize and quantify AD pathophysiology. By showing that GWR is associated with cortical thickness as well as tau deposition, even after controlling for cortical thickness, we argue that GWR is a uniquely sensitive *in vivo* marker of neurodegenerative change reflecting pathological mechanisms that may occur prior to cortical atrophy. By using all of these imaging biomarkers of AD together, we may be better able to capture, and possibly predict, AD neuropathologic changes *in vivo*. We hope that such an approach will ultimately contribute to better endpoints to evaluate the efficacy of therapeutic interventions as we move toward an era of disease-modifying treatments for this devastating disease.

CRediT authorship contribution statement

Deepti Putcha: Conceptualization, Methodology, Formal analysis, Writing – original draft, Visualization, Project administration. **Yuta Katsumi:** Methodology, Software, Formal analysis, Data curation, Writing – original draft, Visualization. **Michael Brickhouse:** Software, Formal analysis, Investigation, Data curation, Visualization. **Ryn Flaherty:** Formal analysis, Investigation, Data curation. **David H. Salat:** Methodology, Writing – review & editing. **Alexandra Touroutoglou:** Conceptualization, Methodology, Writing – review & editing, Visualization, Supervision, Project administration. **Bradford C. Dickerson:** Conceptualization, Methodology, Resources, Writing – review & editing, Visualization, Supervision, Project administration, Funding acquisition.

Declaration of Competing Interest

The authors declare that they have no known competing financial interests or personal relationships that could have appeared to influence the work reported in this paper.

Data availability

Data will be made available upon reasonable request.

Acknowledgements

The authors would like to thank the patients and families who participated in this research, without whose partnership this research would not have been possible.

Funding

This research was supported by NIH grants K23AG065450, K23DC016912, R21AG051987, R01DC014296, P50AG005134, and P30AG062421. This research was carried out in part at the Athinoula A. Martinos Center for Biomedical Imaging at the MGH, using resources provided by the Center for Functional Neuroimaging Technologies, P41EB015896, a P41 Biotechnology Resource Grant supported by the National Institute of Biomedical Imaging and Bioengineering (NIBIB), National Institutes of Health. This work also involved the use of instrumentation supported by the NIH Shared Instrumentation Grant Program and/or High-End Instrumentation Grant Program; specifically, grant number(s) S10RR021110, S10RR023043, S10RR023401.

Competing interests

Dr. Dickerson has been a consultant for Acadia, Alector, Arkuda, Biogen, Denali, Genentech, Lilly, Merck, Novartis, Takeda, Wave Lifesciences, and has received royalties from Cambridge University Press, Elsevier, Oxford University Press.

Appendix A. Supplementary data

Supplementary data to this article can be found online at https://doi.org/10.1016/j.nicl.2022.103303.

References

Bates, D., Mächler, M., Bolker, B., & Walker, S. (2015). Fitting Linear Mixed-Effects Models Using lme4. *Journal of Statistical Software*, *67*(1), Article 1. 10.18637/jss.v067.i01.

Becker, J.A., Hedden, T., Carmasin, J., Maye, J., Rentz, D.M., Putcha, D., Fischl, B., Greve, D.N., Marshall, G.A., Salloway, S., Marks, D., Buckner, R.L., Sperling, R.A., Johnson, K.A., 2011. Amyloid-β associated cortical thinning in clinically normal elderly. Ann. Neurol. 69 (6), 1032–1042. https://doi.org/10.1002/ana.22333.

Brenowitz, W.D., Keene, C.D., Hawes, S.E., Hubbard, R.A., Longstreth, W.T., Woltjer, R.L., Crane, P.K., Larson, E.B., Kukull, W.A., 2017. Alzheimer's disease neuropathologic change, Lewy body disease, and vascular brain injury in clinic- and community-based samples. Neurobiol. Aging 53, 83–92. https://doi.org/10.1016/j.neurobiolaging.2017.01.017.

Crutch, S.J., Schott, J.M., Rabinovici, G.D., Murray, M., Snowden, J.S., van der Flier, W.M., Dickerson, B.C., Vandenberghe, R., Ahmed, S., Bak, T.H., Boeve, B.F., Butler, C., Cappa, S.F., Ceccaldi, M., de Souza, L.C., Dubois, B., Felician, O., Galasko, D., Graff-Radford, J., Fox, N.C., 2017. Consensus classification of posterior cortical atrophy. Alzheimer's Dementia 13 (8), 870–884. https://doi.org/10.1016/j.jalz.2017.01.014.

Day, G.S., Gordon, B.A., Jackson, K., Christensen, J.J., Rosana Ponisio, M., Su, Y., Ances, B.M., Benzinger, T.L.S., Morris, J.C., 2017. Tau-PET binding distinguishes patients with early-stage posterior cortical atrophy from amnestic Alzheimer disease dementia. Alzheimer Dis. Assoc. Disord. 31 (2), 87–93. https://doi.org/10.1097/WAD.0000000000000196.

Desikan, R.S., Ségonne, F., Fischl, B., Quinn, B.T., Dickerson, B.C., Blacker, D., Buckner, R.L., Dale, A.M., Maguire, R.P., Hyman, B.T., Albert, M.S., Killiany, R.J., 2006. An automated labeling system for subdividing the human cerebral cortex on MRI scans into gyral based regions of interest. Neuroimage 31 (3), 968–980. https://doi.org/10.1016/j.neuroimage.2006.01.021.

Dickerson, B.C., Bakkour, A., Salat, D.H., Feczko, E., Pacheco, J., Greve, D.N., Grodstein, F., Wright, C.I., Blacker, D., Rosas, H.D., Sperling, R.A., Atri, A., Growdon, J.H., Hyman, B.T., Morris, J.C., Fischl, B., Buckner, R.L., 2009. The cortical signature of Alzheimer's disease: regionally specific cortical thinning relates to symptom severity in very mild to mild AD dementia and is detectable in asymptomatic amyloid-positive individuals. Cereb. Cortex 19 (3), 497–510. https://doi.org/10.1093/cercor/bhn113.

Dickerson, B.C., McGinnis, S.M., Xia, C., Price, B.H., Atri, A., Murray, M.E., Mendez, M.F., Wolk, D.A., 2017. Approach to atypical Alzheimer's disease and case studies of

the major subtypes. CNS Spectr. 22 (6), 439–449. https://doi.org/10.1017/S109285291600047X.
Fischl, B., Dale, A.M., 2000. Measuring the thickness of the human cerebral cortex from magnetic resonance images. Proc. Natl. Acad. Sci. 97 (20), 11050–11055. https://doi.org/10.1073/pnas.200033797.
Fischl, B., Liu, A., Dale, A.M., 2001. Automated manifold surgery: Constructing geometrically accurate and topologically correct models of the human cerebral cortex. IEEE Trans. Med. Imaging 20 (1), 70–80. https://doi.org/10.1109/42.906426.
Fleisher, A. S., Pontecorvo, M. J., Devous, M. D., Sr, Lu, M., Arora, A. K., Truocchio, S. P., Aldea, P., Flitter, M., Locascio, T., Devine, M., Siderowf, A., Beach, T. G., Montine, T. J., Serrano, G. E., Curtis, C., Perrin, A., Salloway, S., Daniel, M., Wellman, C., … for the A16 Study Investigators. (2020). Positron Emission Tomography Imaging With [18F]flortaucipir and Postmortem Assessment of Alzheimer Disease Neuropathologic Changes. *JAMA Neurology*, *77*(7), 829–839. 10.1001/jamaneurol.2020.0528.
Gómez-Isla, T., Hollister, R., West, H., Mui, S., Growdon, J.H., Petersen, R.C., Parisi, J.E., Hyman, B.T., 1997. Neuronal loss correlates with but exceeds neurofibrillary tangles in Alzheimer's disease. Ann. Neurol. 41 (1), 17–24. https://doi.org/10.1002/ana.410410106.
Gorno-Tempini, M.L., Hillis, A.E., Weintraub, S., Kertesz, A., Mendez, M., Cappa, S.F., Ogar, J.M., Rohrer, J.D., Black, S., Boeve, B.F., Manes, F., Dronkers, N.F., Vandenberghe, R., Rascovsky, K., Patterson, K., Miller, B.L., Knopman, D.S., Hodges, J.R., Mesulam, M.M., Grossman, M., 2011. Classification of primary progressive aphasia and its variants. Neurology 76 (11), 1006–1014. https://doi.org/10.1212/WNL.0b013e31821103e6.
Greve, D.N., Svarer, C., Fisher, P.M., Feng, L., Hansen, A.E., Baare, W., Rosen, B., Fischl, B., Knudsen, G.M., 2014. Cortical surface-based analysis reduces bias and variance in kinetic modeling of brain PET data. Neuroimage 92, 225–236. https://doi.org/10.1016/j.neuroimage.2013.12.021.
Greve, D.N., Salat, D.H., Bowen, S.L., Izquierdo-Garcia, D., Schultz, A.P., Catana, C., Becker, J.A., Svarer, C., Knudsen, G.M., Sperling, R.A., Johnson, K.A., 2016. Different partial volume correction methods lead to different conclusions: An 18F-FDG-PET study of aging. Neuroimage 132, 334–343. https://doi.org/10.1016/j.neuroimage.2016.02.042.
Grydeland, H., Westlye, L.T., Walhovd, K.B., Fjell, A.M., 2013. Improved prediction of Alzheimer's disease with longitudinal white matter/gray matter contrast changes. Hum. Brain Mapp. 34 (11), 2775–2785. https://doi.org/10.1002/hbm.22103.
Hyman, B.T., Phelps, C.H., Beach, T.G., Bigio, E.H., Cairns, N.J., Carrillo, M.C., Dickson, D.W., Duyckaerts, C., Frosch, M.P., Masliah, E., Mirra, S.S., Nelson, P.T., Schneider, J.A., Thal, D.R., Thies, B., Trojanowski, J.Q., Vinters, H.V., Montine, T.J., 2012. National Institute on Aging–Alzheimer's Association guidelines for the neuropathologic assessment of Alzheimer's disease. Alzheimer's Dementia 8 (1), 1–13. https://doi.org/10.1016/j.jalz.2011.10.007.
Jack, C.R., Knopman, D.S., Jagust, W.J., Petersen, R.C., Weiner, M.W., Aisen, P.S., Shaw, L.M., Vemuri, P., Wiste, H.J., Weigand, S.D., Lesnick, T.G., Pankratz, V.S., Donohue, M.C., Trojanowski, J.Q., 2013. Tracking pathophysiological processes in Alzheimer's disease: an updated hypothetical model of dynamic biomarkers. Lancet Neurol. 12 (2), 207–216. https://doi.org/10.1016/S1474-4422(12)70291-0.
Jack, C.R., Bennett, D.A., Blennow, K., Carrillo, M.C., Feldman, H.H., Frisoni, G.B., Hampel, H., Jagust, W.J., Johnson, K.A., Knopman, D.S., Petersen, R.C., Scheltens, P., Sperling, R.A., Dubois, B., 2016. A/T/N: an unbiased descriptive classification scheme for Alzheimer disease biomarkers. Neurology 87 (5), 539–547. https://doi.org/10.1212/WNL.0000000000002923.
Jack, C.R., Bennett, D.A., Blennow, K., Carrillo, M.C., Dunn, B., Haeberlein, S.B., Holtzman, D.M., Jagust, W., Jessen, F., Karlawish, J., Liu, E., Molinuevo, J.L., Montine, T., Phelps, C., Rankin, K.P., Rowe, C.C., Scheltens, P., Siemers, E., Snyder, H.M., Silverberg, N., 2018. NIA-AA research framework: toward a biological definition of Alzheimer's disease. Alzheimer's Dementia 14 (4), 535–562. https://doi.org/10.1016/j.jalz.2018.02.018.
Jefferson, A.L., Gifford, K.A., Damon, S., Chapman, G.W., Liu, D., Sparling, J., Dobromyslin, V., Salat, D., for the Alzheimer's Disease Neuroimaging Initiative, 2015. Gray & white matter tissue contrast differentiates Mild Cognitive Impairment converters from non-converters. Brain Imag. Behav. 9 (2), 141–148. https://doi.org/10.1007/s11682-014-9291-2.
Johnson, K.A., Schultz, A., Betensky, R.A., Becker, J.A., Sepulcre, J., Rentz, D., Mormino, E., Chhatwal, J., Amariglio, R., Papp, K., Marshall, G., Albers, M., Mauro, S., Pepin, L., Alverio, J., Judge, K., Philiossaint, M., Shoup, T., Yokell, D., Sperling, R., 2016. Tau positron emission tomographic imaging in aging and early Alzheimer disease. Ann. Neurol. 79 (1), 110–119. https://doi.org/10.1002/ana.24546.
Katsumi, Y., Putcha, D., Eckbo, R., Wong, B., Quimby, M., McGinnis, S., Touroutoglou, A., Dickerson, B.C., 2022a. Anterior dorsal attention network tau drives visual attention deficits in posterior cortical atrophy. Brain awac245. https://doi.org/10.1093/brain/awac245.
Katsumi, Y., Quimby, M., Hochberg, D., Jones, A., Brickhouse, M., Eldaief, M.C., Dickerson, B.C., Touroutoglou, A., 2022b. Association of regional cortical network atrophy with progression to dementia in patients with primary progressive aphasia. Neurology. https://doi.org/10.1212/WNL.0000000000201403.
Kljajevic, V., Grothe, M.J., Ewers, M., Teipel, S., 2014. Distinct pattern of hypometabolism and atrophy in preclinical and predementia Alzheimer's disease. Neurobiol. Aging 35 (9), 1973–1981. https://doi.org/10.1016/j.neurobiolaging.2014.04.006.
Mendez, M.F., Ghajarania, N., Perryman, K.M., 2002. Posterior cortical atrophy: clinical characteristics and differences compared to Alzheimer's disease. Dement. Geriatr. Cogn. Disord. 14 (1), 33–40.
Nasreddine, Z.S., Phillips, N.A., Bédirian, V., Charbonneau, S., Whitehead, V., Collin, I., Cummings, J.L., Chertkow, H., 2005. The Montreal Cognitive Assessment, MoCA: a brief screening tool for mild cognitive impairment. J. Am. Geriatr. Soc. 53 (4), 695–699. https://doi.org/10.1111/j.1532-5415.2005.53221.x.
Ossenkoppele, R., Pijnenburg, Y.A.L., Perry, D.C., Cohn-Sheehy, B.I., Scheltens, N.M.E., Vogel, J.W., Kramer, J.H., van der Vlies, A.E., Joie, R.L., Rosen, H.J., van der Flier, W.M., Grinberg, L.T., Rozemuller, A.J., Huang, E.J., van Berckel, B.N.M., Miller, B.L., Barkhof, F., Jagust, W.J., Scheltens, P., Rabinovici, G.D., 2015. The behavioural/dysexecutive variant of Alzheimer's disease: Clinical, neuroimaging and pathological features. Brain 138 (9), 2732–2749. https://doi.org/10.1093/brain/awv191.
Putcha, D., McGinnis, S.M., Brickhouse, M., Wong, B., Sherman, J.C., Dickerson, B.C., 2018. Executive dysfunction contributes to verbal encoding and retrieval deficits in posterior cortical atrophy. Cortex 106, 36–46. https://doi.org/10.1016/j.cortex.2018.04.010.
Putcha, D., Brickhouse, M., Touroutoglou, A., Collins, J.A., Quimby, M., Wong, B., Eldaief, M., Schultz, A., El Fakhri, G., Johnson, K., Dickerson, B.C., McGinnis, S.M., 2019. Visual cognition in non-amnestic Alzheimer's disease: relations to tau, amyloid, and cortical atrophy. NeuroImage: Clinical 23, 101889. https://doi.org/10.1016/j.nicl.2019.101889.
Putcha, D., Eckbo, R., Katsumi, Y., Dickerson, B.C., Touroutoglou, A., Collins, J.A., 2022. Tau and the fractionated default mode network in atypical Alzheimer's disease. Brain Commun. 4 (2), fcac055. https://doi.org/10.1093/braincomms/fcac055.
Rabinovici, G.D., Furst, A.J., Alkalay, A., Racine, C.A., O'Neil, J.P., Janabi, M., Baker, S. L., Agarwal, N., Bonasera, S.J., Mormino, E.C., Weiner, M.W., Gorno-Tempini, M.L., Rosen, H.J., Miller, B.L., Jagust, W.J., 2010. Increased metabolic vulnerability in early-onset Alzheimer's disease is not related to amyloid burden. Brain 133 (2), 512–528. https://doi.org/10.1093/brain/awp326.
Rabinovici, G.D., Rosen, H.J., Alkalay, A., Kornak, J., Furst, A.J., Agarwal, N., Mormino, E.C., O'Neil, J.P., Janabi, M., Karydas, A., Growdon, M.E., Jang, J.Y., Huang, E.J., DeArmond, S.J., Trojanowski, J.Q., Grinberg, L.T., Gorno-Tempini, M. L., Seeley, W.W., Miller, B.L., Jagust, W.J., 2011. Amyloid vs FDG-PET in the differential diagnosis of AD and FTLD. Neurology 77 (23), 2034–2042. https://doi.org/10.1212/WNL.0b013e31823b9c5e.
Salat, D.H., Lee, S.Y., van der Kouwe, A.J., Greve, D.N., Fischl, B., Rosas, H.D., 2009. Age-associated alterations in cortical gray and white matter signal intensity and gray to white matter contrast. Neuroimage 48 (1), 21–28. https://doi.org/10.1016/j.neuroimage.2009.06.074.
Salat, D.H., Chen, J.J., van der Kouwe, A.J., Greve, D.N., Fischl, B., Rosas, H.D., 2011. Hippocampal degeneration is associated with temporal and limbic gray matter/white matter tissue contrast in Alzheimer's disease. Neuroimage 54 (3), 1795–1802. https://doi.org/10.1016/j.neuroimage.2010.10.034.
Sapolsky, D., Bakkour, A., Negreira, A., Nalipinski, P., Weintraub, S., Mesulam, M.-M., Caplan, D., Dickerson, B.C., 2010. Cortical neuroanatomic correlates of symptom severity in primary progressive aphasia. Neurology 75 (4), 358–366. https://doi.org/10.1212/WNL.0b013e3181ea15e8.
Schaefer, A., Kong, R., Gordon, E.M., Laumann, T.O., Zuo, X.-N., Holmes, A.J., Eickhoff, S.B., Yeo, B.T.T., 2018. Local-global parcellation of the human cerebral cortex from intrinsic functional connectivity MRI. Cereb. Cortex 28 (9), 3095–3114. https://doi.org/10.1093/cercor/bhx179.
Shoup, T.M., Yokell, D.L., Rice, P.A., Jackson, R.N., Livni, E., Johnson, K.A., Brady, T.J., Vasdev, N., 2013. A concise radiosynthesis of the tau radiopharmaceutical, [18F] T807. J. Label. Compd. Radiopharm. 56 (14), 736–740. https://doi.org/10.1002/jlcr.3098.
Sintini, I., Martin, P.R., Graff-Radford, J., Senjem, M.L., Schwarz, C.G., Machulda, M.M., Spychalla, A.J., Drubach, D.A., Knopman, D.S., Petersen, R.C., Lowe, V.J., Jack, C.R., Josephs, K.A., Whitwell, J.L., 2019. Longitudinal tau-PET uptake and atrophy in atypical Alzheimer's disease. NeuroImage: Clinical 23, 101823. https://doi.org/10.1016/j.nicl.2019.101823.
Sonni, I., Lesman Segev, O.H., Baker, S.L., Iaccarino, L., Korman, D., Rabinovici, G.D., Jagust, W.J., Landau, S.M., La Joie, R., for the A. D. N. I., 2020. Evaluation of a visual interpretation method for tau-PET with 18F-flortaucipir. Alzheimer's Dementia: Diagn. Assess. Dis. Monit. 12 (1), e12133.
Spotorno, N., Strandberg, O., Vis, G., Stomrud, E., Nilsson, M., Hansson, O., 2022. Measures of cortical microstructure are linked to amyloid pathology in Alzheimer's disease. Brain awac343. https://doi.org/10.1093/brain/awac343.
Tang-Wai, D.F., Graff-Radford, N.R., Boeve, B.F., Dickson, D.W., Parisi, J.E., Crook, R., Caselli, R.J., Knopman, D.S., Petersen, R.C., 2004. Clinical, genetic, and neuropathologic characteristics of posterior cortical atrophy. Neurology.
Townley, R.A., Graff-Radford, J., Mantyh, W.G., Botha, H., Polsinelli, A.J., Przybelski, S. A., Machulda, M.M., Makhlouf, A.T., Senjem, M.L., Murray, M.E., Reichard, R.R., Savica, R., Boeve, B.F., Drubach, D.A., Josephs, K.A., Knopman, D.S., Lowe, V.J., Jack Jr, C.R., Petersen, R.C., Jones, D.T., 2020. Progressive dysexecutive syndrome due to Alzheimer's disease: a description of 55 cases and comparison to other phenotypes. Brain Commun. 2 (1), fcaa068. https://doi.org/10.1093/braincomms/fcaa068.
Villeneuve, S., Rabinovici, G.D., Cohn-Sheehy, B.I., Madison, C., Ayakta, N., Ghosh, P.M., La Joie, R., Arthur-Bentil, S.K., Vogel, J.W., Marks, S.M., Lehmann, M., Rosen, H.J., Reed, B., Olichney, J., Boxer, A.L., Miller, B.L., Borys, E., Jin, L.-W., Huang, E.J., Jagust, W., 2015. Existing Pittsburgh Compound-B positron emission tomography thresholds are too high: statistical and pathological evaluation. Brain 138 (7), 2020–2033. https://doi.org/10.1093/brain/awv112.
Westlye, L.T., Walhovd, K.B., Dale, A.M., Espeseth, T., Reinvang, I., Raz, N., Agartz, I., Greve, D.N., Fischl, B., Fjell, A.M., 2009. Increased sensitivity to effects of normal aging and Alzheimer's disease on cortical thickness by adjustment for local

variability in gray/white contrast: a multi-sample MRI study. Neuroimage 47 (4), 1545–1557. https://doi.org/10.1016/j.neuroimage.2009.05.084.

Westlye, L.T., Walhovd, K.B., Dale, A.M., Bjørnerud, A., Due-Tønnessen, P., Engvig, A., Grydeland, H., Tamnes, C.K., Østby, Y., Fjell, A.M., 2010. Differentiating maturational and aging-related changes of the cerebral cortex by use of thickness and signal intensity. Neuroimage 52 (1), 172–185. https://doi.org/10.1016/j.neuroimage.2010.03.056.

Whitwell, J.L., Graff-Radford, J., Tosakulwong, N., Weigand, S.D., Machulda, M.M., Senjem, M.L., Spychalla, A.J., Vemuri, P., Jones, D.T., Drubach, D.A., Knopman, D. S., Boeve, B.F., Ertekin-Taner, N., Petersen, R.C., Lowe, V.J., Jack Jr., C.R., Josephs, K.A., 2018. Imaging correlations of tau, amyloid, metabolism, and atrophy in typical and atypical Alzheimer's disease. Alzheimer's Dementia 14 (8), 1005–1014. https://doi.org/10.1016/j.jalz.2018.02.020.

Wirth, M., Madison, C.M., Rabinovici, G.D., Oh, H., Landau, S.M., Jagust, W.J., 2013. Alzheimer's Disease Neurodegenerative Biomarkers Are Associated with Decreased Cognitive Function but Not β-Amyloid in Cognitively Normal Older Individuals. J. Neurosci. 33 (13), 5553–5563. https://doi.org/10.1523/JNEUROSCI.4409-12.2013.

Wong, B., Lucente, D.E., MacLean, J., Padmanabhan, J., Quimby, M., Brandt, K.D., Putcha, D., Sherman, J., Frosch, M.P., McGinnis, S., Dickerson, B.C., 2019. Diagnostic evaluation and monitoring of patients with posterior cortical atrophy. Neurodegen. Disease Manage. 9 (4), 217–239. https://doi.org/10.2217/nmt-2018-0052.

Xia, C., Makaretz, S.J., Caso, C., McGinnis, S., Gomperts, S.N., Sepulcre, J., Gomez-Isla, T., Hyman, B.T., Schultz, A., Vasdev, N., Johnson, K.A., Dickerson, B.C., 2017. Association of In Vivo [18F]AV-1451 Tau PET imaging results with cortical atrophy and symptoms in typical and atypical Alzheimer disease. JAMA Neurol. 74 (4), 427. https://doi.org/10.1001/jamaneurol.2016.5755.

Yeo, B.T.T., Krienen, F.M., Sepulcre, J., Sabuncu, M.R., Lashkari, D., Hollinshead, M., Roffman, J.L., Smoller, J.W., Zöllei, L., Polimeni, J.R., Fischl, B., Liu, H., Buckner, R. L., 2011. The organization of the human cerebral cortex estimated by intrinsic functional connectivity. J. Neurophysiol. 106 (3), 1125–1165. https://doi.org/10.1152/jn.00338.2011.